

Vortex Reconnection or Breakdown Subsequent to Perpendicular Collision With a Solid Body

Larry A. Young
 Aerospace Engineer
 (650)-604-4022
 NASA Ames Research Center
 Moffett Field, CA 94035

Summary

This paper analytically examines the unsteady fluid dynamics of a vortex filament subsequent to a normal collision of the vortex with a solid body. In particular, the breakdown or reconnection phenomena, post-collision, for a vortex filament is studied. The paper does not investigate the collision dynamics process itself. The derived exact solution is based upon the laminar viscous form of the Helmholtz equations.

Nomenclature

- r Radial coordinate, origin at filament axis, ft
 r^* Nondimensional radial coordinate, $r^*=r/s$
 r_c Vortex filament core size radii as a function of time, t, ft
 Re Vortex filament Reynolds number, $Re = \gamma/\nu$

Paper to be presented at 30'th AIAA Fluid Dynamics Conference, Norfolk, VA, June 28-July 1, 1999. Conference Technical Topic: Vortex Dynamics.

- s Axial distance of filament breakpoint (time equal zero) from origin, ft
- t Time, sec
- t^* Nondimensional time parameter, $t^*=vt/s^2$
- \mathbf{V} Velocity vector, cylindrical coordinates, $\mathbf{V}=[v_r \ v_\theta \ v_z]$, ft/sec
- v_r Radial velocity component, ft/sec
- v_r^* Nondimensional radial velocity component
- v_z Axial (along vortex filament axis) velocity component, ft/sec
- v_z^* Nondimensional axial velocity component
- v_θ Tangential velocity component, ft/sec
- v_θ^* Nondimensional tangential velocity component
- z Axial (along vortex filament axis) coordinate, origin at intersection of filament segments' plane of symmetry and filament axis, ft
- z^* Nondimensional axial coordinate, $z^*=z/s$
- γ Vortex filament initial circulation strength, ft²/sec
- Γ Vortex circulation, ft²/sec
- ν Kinematic viscosity, ft²/sec
- θ Angular coordinate, radians
- ω Vorticity vector, $\omega=[\omega_r \ \omega_\theta \ \omega_z]$, ft²/sec
- ψ^* Quasi-stream function

Introduction

Vortex filament 'collisions' with solid bodies occur in a number of real world examples for rotary-wing aircraft: blade vortex interactions where vortices shed from one blade collide with another blade; trailed tip vortex interactions/collisions with a helicopter airframe/tailboom in hover and low-speed flight; or, alternatively, proprotor trailed tip vortex collisions with wing surfaces for tiltrotor aircraft in airplane-mode. For, blade vortex interactions, references 1-3 provide qualitative discussion regarding the vortex filament collision process. References 4-7 provide a similar qualitative discussion of vortex fuselage/airframe/wing collisions.

Very little work to date has been performed examining the post-collision dynamics of vortex/solid body interactions. Most work has either concentrated on the collision process itself (see reference 8) or, alternatively, has looked at vortex-on-vortex collisions (see reference 9, for example). A related academic exercise is the study of ring vortices throughout the collision process; see reference 10, for example.

Nonetheless, flow visualization techniques are sufficiently maturing so as to examine in detail the rotary-wing/airframe vortex filament collision process - see, in particular, references 4, 5, and 7. It's clear that current rotor wake CFD analyses are inadequate to represent rotor vortex filament collision and subsequent breakdown or reconnection. This paper proposes as a initial step towards understanding the very complex flow phenomena of rotor wakes a first order analytical treatment of the vortex filament/solid body collision process. This paper will concentrate on the post-collision vortex filament fluid dynamics.

Problem Description

Figure 1 illustrates the point that there is going to be varying degrees of vortex filament breakage (in form of filament distortion and separation of breakpoints) depending on the severity of the collision process. Vortex filament collisions with thin solid bodies will tend to minimize the separation distance between the filament segment breakpoints as well as minimize the filament distortion. Therefore, collision with thin solid bodies will tend to result in the 'reconnection' of the vortex filaments. Conversely, collisions with bluff bodies will tend to result in large breakpoint separation distances and considerable filament segment distortion -- therefore, most likely resulting in filament segment 'breakdown.'

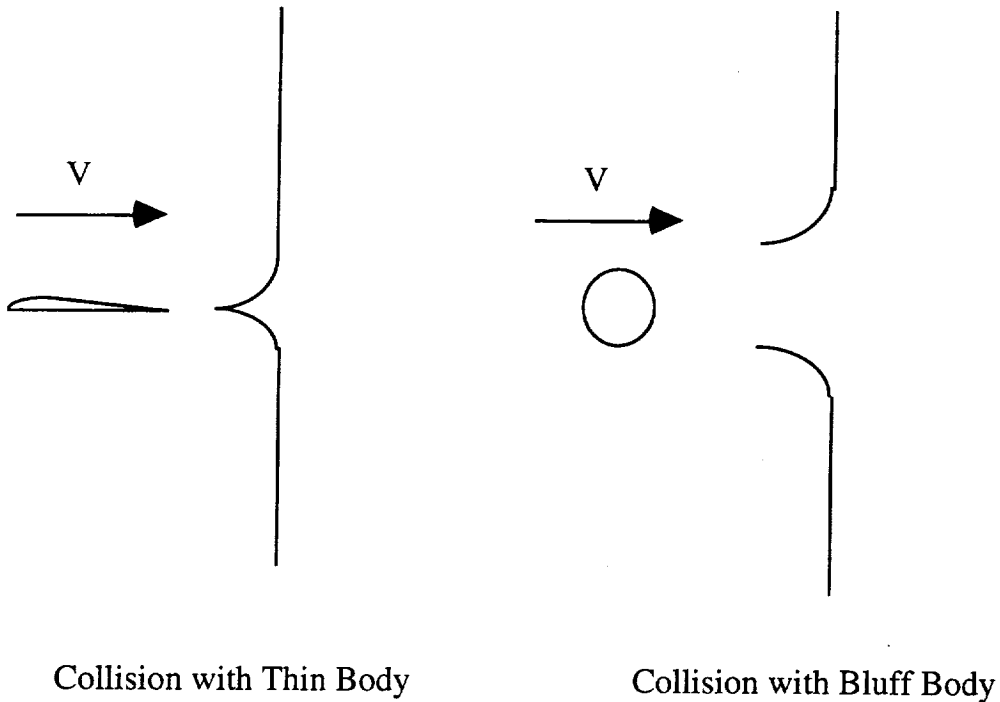


Figure 1 - Hypothetical Vortex Filament Distortion/Breakage After Collision with Solid Bodies

Figure 2 illustrates an idealized version of the vortex filament in the intermediate process of vortex reconnection/breakdown, post-collision. Distortion of the filament as to deflection of filament axis laterally from its undisturbed orientation is neglected. Initial axial flow (along the filament) is assumed to be zero as a result of the collision process: the filament, as it wraps around the solid body, will have to obey the no-flow boundary constraint.

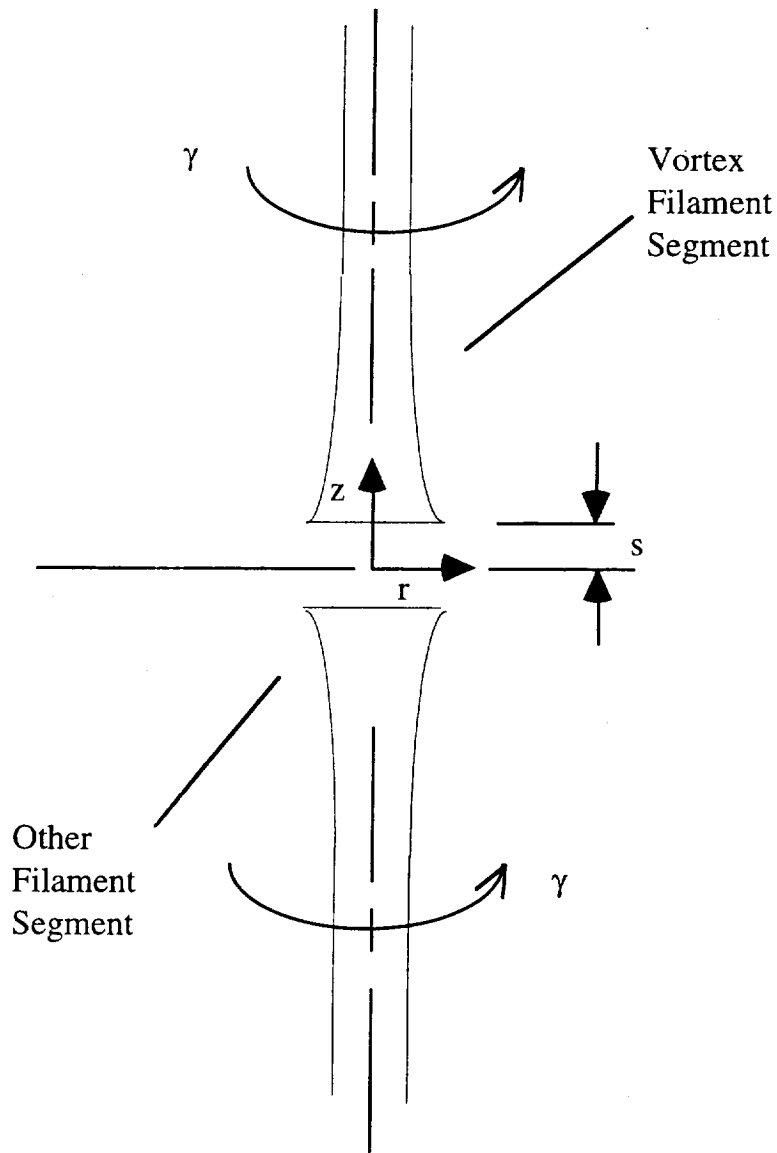


Figure 2 - Vortex Geometry Description. (Vortex Filament Described by Contour of Maximum Velocity)

Governing Equations

The Helmholtz equation for laminar-flow vorticity (references 13 and 14) is given by

$$\frac{D\omega}{Dt} = (\omega \cdot \nabla)\mathbf{V} + \nu \nabla^2 \omega \quad (1)$$

The term $D\omega/Dt$ is the 'particle derivative' for the vorticity. And, further, (references 13 and 14)

$$\text{div} \omega \equiv \nabla \cdot \omega = 0 \quad (2)$$

where

$$\omega = \text{curl} \mathbf{V} = \nabla \times \mathbf{V} \quad (3)$$

Considering the vorticity component about the z-axis (ω_z), for the problem under discussion -- and using the cylindrical coordinate system for the Helmholtz, vorticity divergence equations, and the vorticity definition -- the above two equations become respectively

$$\begin{aligned} \frac{\partial \omega_z}{\partial t} + v_r \frac{\partial \omega_z}{\partial r} + \frac{v_\theta}{r} \frac{\partial \omega_z}{\partial \theta} + v_z \frac{\partial \omega_z}{\partial z} = \\ \omega_r \frac{\partial v_z}{\partial r} + \frac{\omega_\theta}{r} \frac{\partial v_z}{\partial \theta} + \omega_z \frac{\partial v_z}{\partial z} + \nu \left\{ \frac{\partial^2 \omega_z}{\partial r^2} + \frac{1}{r} \frac{\partial \omega_z}{\partial r} + \frac{1}{r^2} \frac{\partial^2 \omega_z}{\partial \theta^2} + \frac{\partial^2 \omega_z}{\partial z^2} \right\} \end{aligned} \quad (4)$$

$$\frac{1}{r} \frac{\partial}{\partial r} (r \omega_r) + \frac{1}{r} \frac{\partial \omega_\theta}{\partial \theta} + \frac{\partial \omega_z}{\partial z} = 0 \quad (5)$$

where

$$\omega_r = \frac{1}{r} \frac{\partial v_z}{\partial \theta} - \frac{\partial v_\theta}{\partial z}$$

$$\omega_\theta = \frac{\partial v_r}{\partial z} - \frac{\partial v_z}{\partial r}$$

$$\omega_z = \frac{\partial v_\theta}{\partial r} + \frac{v_\theta}{r} - \frac{1}{r} \frac{\partial v_r}{\partial \theta}$$

(6a-c)

Imposing θ -symmetry on equations 4, 5, and 6a-c gives

$$\frac{\partial \omega_z}{\partial t} + v_r \frac{\partial \omega_z}{\partial r} + v_z \frac{\partial \omega_z}{\partial z} = \omega_r \frac{\partial v_z}{\partial r} + \omega_z \frac{\partial v_z}{\partial z} + v \left\{ \frac{\partial^2 \omega_z}{\partial r^2} + \frac{1}{r} \frac{\partial \omega_z}{\partial r} + \frac{\partial^2 \omega_z}{\partial z^2} \right\} \quad (7)$$

$$\omega_z = - \int \left(\frac{\partial \omega_r}{\partial r} + \frac{\omega_r}{r} \right) dz \quad (8)$$

where

$$\omega_r = - \frac{\partial v_\theta}{\partial z}$$

$$\omega_{\theta} = \frac{\partial v_r}{\partial z} - \frac{\partial v_z}{\partial r}$$

$$\omega_z = \frac{\partial v_{\theta}}{\partial r} + \frac{v_{\theta}}{r}$$

(9a-c)

Note that substitution of equation 9a into equation 8 automatically satisfies equation 9c. Finally, the continuity equation (θ -symmetry) requires that

$$\frac{1}{r} \frac{\partial}{\partial r}(rv_r) + \frac{1}{r} \frac{\partial v_{\theta}}{\partial \theta} + \frac{\partial v_z}{\partial z} \rightarrow \frac{v_r}{r} + \frac{\partial v_r}{\partial r} + \frac{\partial v_z}{\partial z} = 0 \quad (10)$$

Or, rather

$$v_z = -\int \left\{ \frac{\partial v_r}{\partial r} + \frac{v_r}{r} \right\} dz \quad (11)$$

This completes the set of required governing equations necessary to solve the described problem for laminar flow.

Solution

A class of unsteady laminar flow problems called 'moving boundary' problems has been exhaustively studied in the literature. By assuming that $v_r=v_z=0$, the Navier-Stokes equations (or, correspondingly, the Helmholtz vorticity equation) can be reduced to the well-known unsteady heat conduction equation (reference 15).

The Lamb-Oseen vortex solution (references 13 and 14) is one member of this class of unsteady laminar flow problems.

What is sought then is a new class of flow problems that not only encompasses the 'moving boundary' class of problems but the problem described in this paper. But key to defining this new class of flow problems remains the mathematical challenge of reducing the Helmholtz equation, with θ -symmetry, to the unsteady heat conduction equation.

It is proposed that this new class of solution can be defined by assuming that the radial velocity component, v_r , is not merely equal to zero but instead is proportional to the tangential velocity gradient with respect to the z -axis (equation 12). (Note that if the tangential velocity gradient is zero, such as in the case of the Lamb-Oseen vortex, then the 'moving boundary' class of problems is recaptured.)

$$v_r \propto \frac{\partial v_\theta}{\partial z} \quad (12a)$$

Or

$$v_r = \ell \frac{\partial v_\theta}{\partial z} \quad (12b)$$

Where the length scale factor, ℓ , is a constant that transforms the proportional relationship of equation 12a to the equivalence relationship of 12b. (The constant ℓ has the unit of length - hence it being called a 'length scale factor.')

This will be discussed in detail later in the paper.

Meanwhile, continuing with the analysis with the proportional relationship for radial velocity, applying equation 12a to equation 11 gives a second proportional relationship based on flow continuity for the axial velocity.

$$v_z \propto -\left(\frac{\partial v_\theta}{\partial r} + \frac{v_\theta}{r}\right) \quad (13)$$

Applying equations 12a and 13 to equations 9a-c gives

$$\omega_r \propto -v_r$$

$$\omega_z \propto -v_z$$

(14a-b)

Application of equations 12a, 13, and 14a-b to equation 7 causes the convective acceleration terms to cancel out the vortex stretching terms and thereby achieves the objective of reducing the Helmholtz equation to the unsteady heat conduction equation (equation 15).

$$\frac{\partial \omega_z}{\partial t} = v \left\{ \frac{\partial^2 \omega_z}{\partial r^2} + \frac{1}{r} \frac{\partial \omega_z}{\partial r} + \frac{\partial^2 \omega_z}{\partial z^2} \right\} \quad (15)$$

Reference 15 reveals that a particular solution of equation 15, for a instantaneous point source, is given by

$$\omega_z|_{\text{point source}} = \frac{c}{8(\pi vt)^{3/2}} e^{-(r^2 + (z-z_*)^2)/4vt} \quad (16)$$

where c is a constant, z_* is the origin of the instantaneous point source with respect to the z -axis, and r and z are the coordinates of the point for which the vorticity is predicted.

Correspondingly, reference 15 derives the solution to the unsteady heat conduction equation for an instantaneous line source of infinite length (represented as a continuous distribution of instantaneous point sources) by the equation 17.

$$\begin{aligned}\omega_z|_{\text{infinite line source}} &= \frac{c}{8(\pi vt)^{3/2}} \int_{-\infty}^{\infty} e^{-(r^2+(z-z_*)^2)/4vt} dz_* \\ &= \frac{c}{4\pi vt} e^{-r^2/4vt}\end{aligned}\quad (17)$$

With the constant, c , set equal to the circulation strength, γ , (reference 14), then equation 17 becomes the vorticity distribution for a Lamb-Oseen vortex.

To solve the unsteady laminar flow problem for a rectilinear vortex filament that has been 'cut' or 'broken,' however, it is necessary to represent the vortex filament segments with semi-infinite distributions of instantaneous point sources (equation 18). Note that the constant, c , still has been assigned the value $c=\gamma$.

$$\omega_z = \frac{\gamma}{8(\pi vt)^{3/2}} e^{-r^2/4vt} \left\{ \int_s^{\infty} e^{-(z-z_*)^2/4vt} dz_* + \int_{-\infty}^{-s} e^{-(z-z_*)^2/4vt} dz_* \right\} \quad (18)$$

The integral terms in equation 18 can be found in standard handbooks for integration formulas (see reference 16). The solution of vorticity component with respect to the z -axis is given by

$$\omega_z = \frac{\gamma}{8\pi vt} e^{-r^2/4vt} \left\{ \operatorname{erfc}\left(\frac{s-z}{\sqrt{4vt}}\right) + \operatorname{erfc}\left(\frac{s+z}{\sqrt{4vt}}\right) \right\} \quad (19)$$

where $\operatorname{erfc}(x)$ is the complementary error function, i.e.,

$$\operatorname{erfc}(x) = \frac{2}{\sqrt{\pi}} \int_x^{\infty} e^{-u^2} du \quad (20)$$

Noting that complementary error function is related to the error function by the relationship $\operatorname{erfc}(x) = 1 - \operatorname{erf}(x)$. And, further, $\operatorname{erf}(-x) = -\operatorname{erf}(x)$, $\operatorname{erf}(\infty) = 1$, and $\operatorname{erf}(0) = 0$. With these properties of the error function and complementary error function in mind, it can be

readily seen that equation 19 satisfies three important boundary constraints and/or conditions.

$$\omega_z \rightarrow \frac{\gamma}{4\pi vt} e^{-r^2/4vt} \quad \text{for} \quad \begin{array}{l} s \rightarrow 0 \\ z \rightarrow \pm\infty \\ t \rightarrow 0 \quad \text{for } |z| \geq s \end{array}$$

(Vorticity distribution approaches that of the Lamb-Oseen Vortex)

Having derived the vorticity distribution, the axial velocity distribution follows straightforwardly from equation 14b, given equation 19.

$$v_z \propto -\frac{\gamma}{8\pi vt} e^{-r^2/4vt} \left\{ \operatorname{erfc}\left(\frac{s-z}{\sqrt{4vt}}\right) + \operatorname{erfc}\left(\frac{s+z}{\sqrt{4vt}}\right) \right\} \quad (21)$$

Having established the proportional relationship $v_z \propto f(r,z,t)$, it is necessary to multiply equation 21 by a length scale to arrive at an equivalence relationship $v_z = \ell f(r,z,t)$. The appropriate length scale factor is the separation distance, i.e., $\ell = \pm s$. Further, specifically, $\ell = +s$ when $z < 0$ and $\ell = -s$ when $z \geq 0$. Besides being a natural length scale factor, using s as the length scale automatically satisfies the 'moving boundary' extreme of the vortex filament breakdown/reconnection problem; i.e., when $s=0$ then $v_z=0$.

$$v_z = -\frac{\gamma s}{8\pi vt} e^{-r^2/4vt} \left\{ \operatorname{erfc}\left(\frac{s-z}{\sqrt{4vt}}\right) + \operatorname{erfc}\left(\frac{s+z}{\sqrt{4vt}}\right) \right\} \quad (22a)$$

where $z < 0$

$$v_z = +\frac{\gamma s}{8\pi vt} e^{-r^2/4vt} \left\{ \operatorname{erfc}\left(\frac{s-z}{\sqrt{4vt}}\right) + \operatorname{erfc}\left(\frac{s+z}{\sqrt{4vt}}\right) \right\} \quad (22b)$$

and where $z > 0$.

Given equations 9c and 19, the tangential velocity distribution can be derived through solution of a first-order ordinary differential equation.

$$v_{\theta} = \frac{\gamma}{2\pi r} \left(1 - e^{-r^2/4vt}\right) \left\{ \operatorname{erfc}\left(\frac{s-z}{\sqrt{4vt}}\right) + \operatorname{erfc}\left(\frac{s+z}{\sqrt{4vt}}\right) \right\} \quad (23)$$

The analogous attributes of equation 23 with respect to the Lamb-Oseen vortex are obvious (reference 14). As demonstrated in a similar manner with respect to the vorticity distribution, if $s \rightarrow 0$ then, correspondingly, the tangential velocity distribution reduces to the Lamb-Oseen profile.

Next, given equations 23 and 12a, the radial velocity, v_r , can be derived by taking the derivative of v_{θ} with respect to z (equation 24).

$$v_r \propto \frac{\gamma}{2\sqrt{\pi^3 vt} \cdot r} \left(1 - e^{-r^2/4vt}\right) \left\{ e^{-(s-z)^2/4vt} - e^{-(s+z)^2/4vt} \right\} \quad (24)$$

Applying the length scale factor, $\ell = \pm s$ (where $\ell = +s$ when $z < 0$ and $\ell = -s$ when $z \geq 0$), to equation 24, given equation 12a, gives the following expression for the radial velocity distribution

$$v_r = + \frac{\gamma s}{2\sqrt{\pi^3 vt} \cdot r} \left(1 - e^{-r^2/4vt}\right) \left\{ e^{-(s-z)^2/4vt} - e^{-(s+z)^2/4vt} \right\} \quad (25a)$$

when $z < 0$,

$$v_r = - \frac{\gamma s}{2\sqrt{\pi^3 vt} \cdot r} \left(1 - e^{-r^2/4vt}\right) \left\{ e^{-(s-z)^2/4vt} - e^{-(s+z)^2/4vt} \right\} \quad (25b)$$

when $z \geq 0$. A key outcome of equations 25a-b is the prediction that the radial velocity is negative (inward to the vortex core) for all values of r , z , and t .

The process and rate by which the vortex filament segments 'reconnect' can be quantified by a single parameter, χ . The derivation of this parameter will now proceed. First, the vortex segment circulation will be defined by equation 26.

$$\Gamma \equiv 2\pi \int_0^r \omega_z r dr \quad (26)$$

Substitution of equation 19 into 26 and performing the required integration yields.

$$\Gamma = \frac{\gamma}{2} (1 - e^{-r^2/4vt}) \left\{ \operatorname{erfc} \left(\frac{s-z}{\sqrt{4vt}} \right) + \operatorname{erfc} \left(\frac{s+z}{\sqrt{4vt}} \right) \right\} \quad (27)$$

See reference 14 for the derivation for the circulation of an infinite line vortex. What is needed to examine the rate of filament segment reconnection is the rate of increase of the circulation in the intermediate region ($z=0$) between filament segments versus the circulation of the filament far away from the breakpoints ($z \rightarrow \pm\infty$). Therefore, the parameter, χ , will be defined as follows

$$\chi \equiv \frac{\Gamma|_{z=0}}{\Gamma|_{z \rightarrow \pm\infty}} \Big|_{r \rightarrow \infty} \quad (28)$$

Application of equation 27 to equation 28 -- taking the appropriate limits for each term in the numerator and denominator of equation 28 -- gives the following expression for χ .

$$\chi = \operatorname{erfc}\left(\frac{s}{\sqrt{4vt}}\right) \quad (29)$$

The implications of equation 29 and equations 22a-b, 23, and 25 of the unsteady flow behavior of the vortex segments will be discussed in the next section of the paper.

Discussion of Results

A set of exact solutions have been derived for the unsteady laminar flow behavior of a vortex filament subsequent to a perpendicular collision with a solid body. A number of simplifying assumptions was required in order to derive this solution. Chief among those assumptions are: (1) that the filament segments still remained straight, parallel, and aligned with each other; (2) a clean 'break' or 'cut' existed such that no initial vortical flow existed in the intermediate region between the breakpoints; (3) implied, but not explicitly assumed, was that the vortex filaments could be represented by a Lamb-Oseen vortex as an initial condition.

Given this set of exact solutions, it is necessary to examine their implications for the vortex filament reconnection (or breakdown) process. In order to examine the results of the above analytical treatment the following dimensionless parameters will need to be defined: $r^* = r/s$; $z^* = z/s$; $t^* = vt/s^2$; $v_r^* = v_r(s/\gamma)$; $v_z^* = v_z(s/\gamma)$; $v_\theta^* = v_\theta(s/\gamma)$.

Figure 3 is the tangential velocity profile with respect to r^* for various values of t^* . The time dependent behavior manifested in figure 3 not only accounts for the Lamb-Oseen vortex viscous diffusion effects but also accounts for viscous vorticity transport from the vortex filament segments ($|z| \geq s$) to the intermediate region ($|z| < s$) between the filament breakpoints.

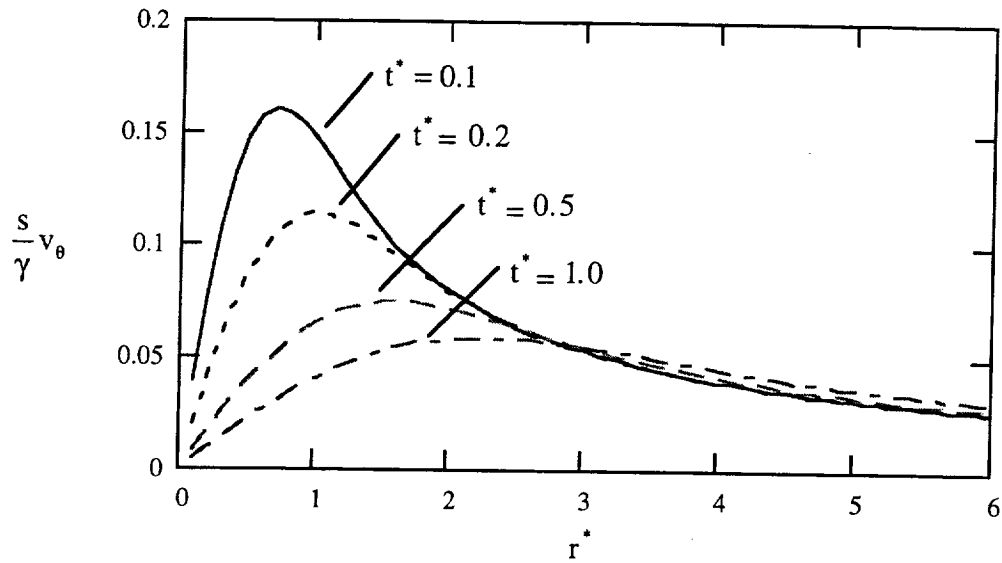


Figure 3 - Tangential Velocity Profile as a Function of Time at the Vortex Filament Breakpoint ($z^*=-1$)

The normalized tangential velocity profile with respect to r^* is similar to the well-recognized Lamb-Oseen tangential vortex profile -- refer to figure 4 - except that the viscous vorticity transport mechanism results in a net reduction in magnitude of the tangential velocities. There are more significant differences in the flow behavior of the reconnecting vortex filament segment problem -- as will be seen.

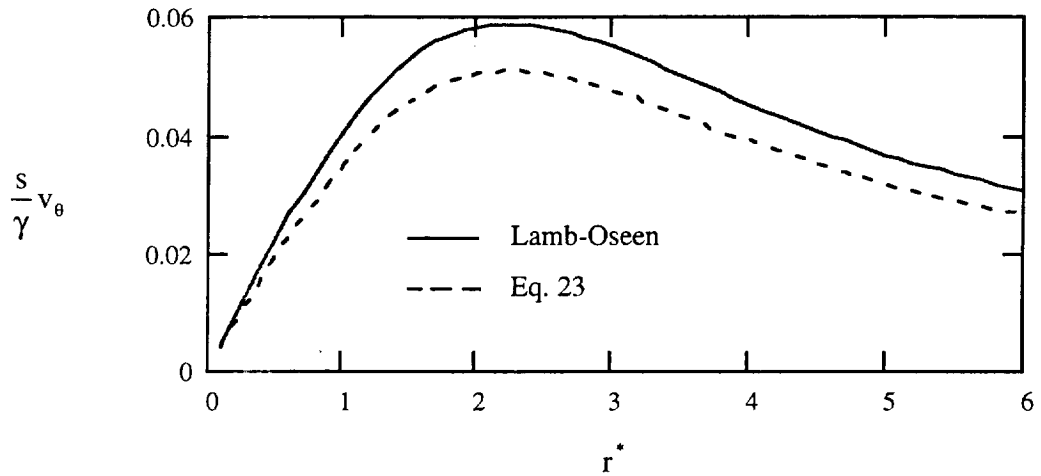


Figure 4 - Differences between the Lamb-Oseen Vortex Tangential Velocity Profile and the Profile for Broken but 'Reconnecting' Filaments ($z^*=-1.0$ and $t^*=1.0$)

As noted earlier, with the Lamb-Oseen vortex , $v_r=v_z=0$. The radial and axial velocities for the 'broken' vortex filament segments are, on the other hand, substantial. Figures 5 and 6a-b illustrate the vortex filament unsteady flow behavior. Figure 5 shows the vector flow field for the r-z plane.

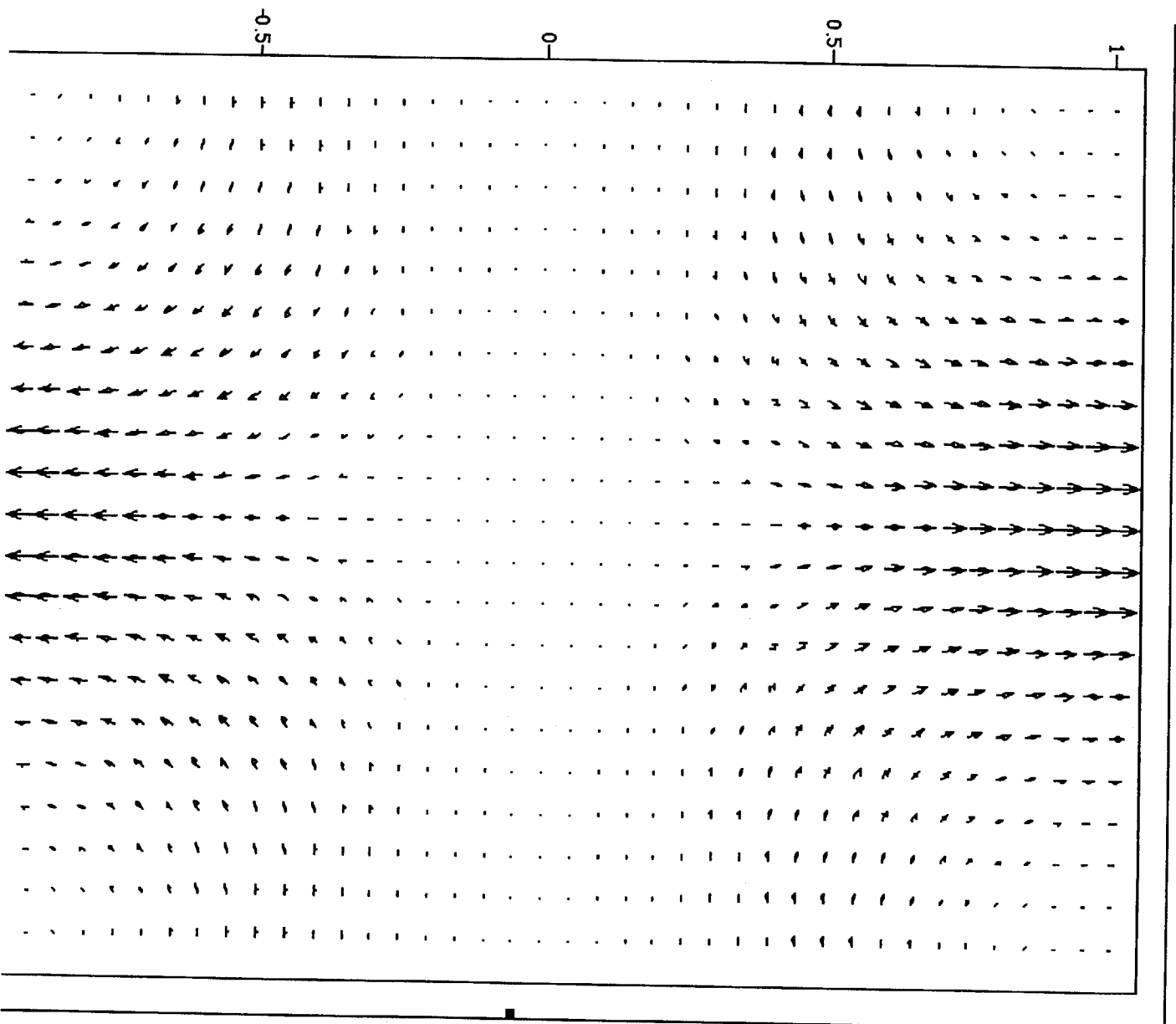


Figure 5 - Vector Field for the r/z Plane ($t^* = 0.1$)

Figure 6a-b are streakline plots for the $r-\theta$ and $r-z$ plane. The key feature of the 'broken' vortex filament unsteady flow are spiral streaklines.

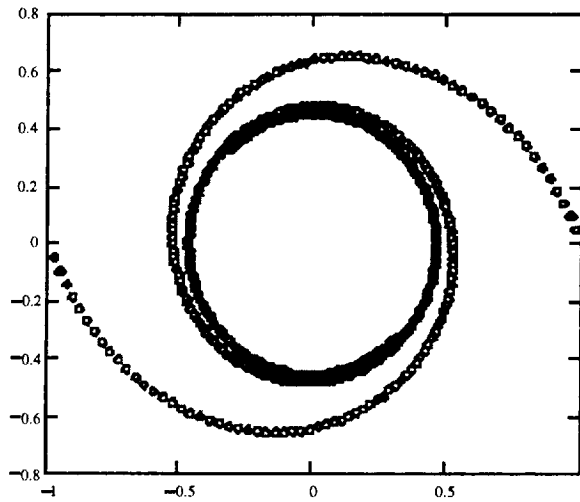


Figure 6a- Streakline Plot for the r-θ Plane

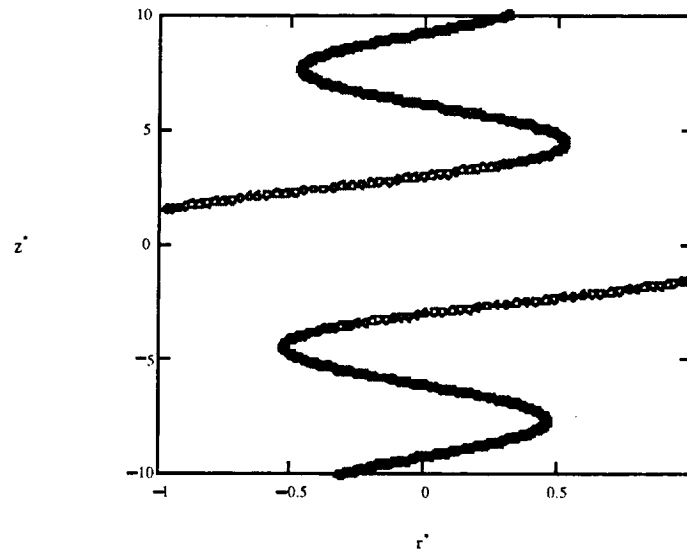


Figure 6b - Streakline Plot for the r-z Plane

The dependence of the parameter χ (equation 29) -- the ratio of circulation of the flow at $z=0$ versus that at $z \rightarrow \pm\infty$ -- with respect to the nondimensionalized time parameter, t^* is shown in figure 7.

Interpretation of figure 7 suggests that the greater than vortex filament breakpoint separation, s , or the lower the kinematic viscosity, ν , the slower (or less likely) the filament reconnection will be accomplished.

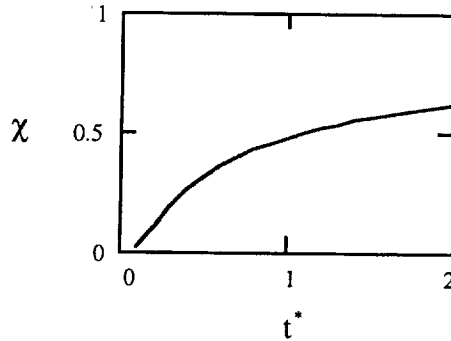


Figure 7 - χ as a function of t^*

There can be no absolute means by which to define when a vortex filament will 'breakdown' versus 'reconnect.' If one were willing to wait an infinite amount of time all broken or cut vortex filaments will eventually reconnect, given one interpretation of equation 29. However, as a practical matter, there will quickly reach a point where the vortex filament segments will have decayed sufficiently via viscous diffusion such that no discernable flow structure will exist by the time reconnection is achieved -- therefore an observer would likely conclude that the vortex filaments have suffered breakdown rather than reconnection. Only some sort of semi-arbitrary criteria can be established to distinguish between vortex filament segment reconnection or breakdown. The author will not propose such a criteria in this paper.

Conclusions

An exact solution for the breakdown or reconnection of a laminar vortex filament -- having been 'cut' or 'broken' subsequent to a collision with a solid body -- has been developed. The analytical solution is based upon the definition of a general class of flow problems that encompasses as a subset the extensively studied 'moving boundary' laminar flow problems. The viscous Helmholtz equation for vorticity is reduced to the unsteady heat conduction equation. Consequently, instantaneous line sources for the vorticity can be used to model the vortex filament breakdown or reconnection process. The analytical solution does not treat, though, the actual collision process itself.

References

1. Spencer, R.H. 'Application of Vortex Visualization Test Techniques to Rotor Noise Research' 26'th Annual Forum of the American Helicopter Society, Philadelphia, PA, June 1970
2. Fontana, R.R. and Hubbard, Jr., J.E. 'A Comparison with Theory of Peak to Peak Sound Level for a Model Helicopter Rotor Generating Blade Slap at Low Tip Speeds' Ninth European Rotorcraft and Powered Lift Aircraft Forum, Stresa, Italy, September 1983
3. Swanson, A.A. 'Application of the Shadowgraph Flow Visualization Technique to a Full-Scale Helicopter Rotor in Hover and Forward Flight' AIAA-93-3411, AIAA 11'th Applied Aerodynamics Conference, Monterey, CA, August, 1993
4. Light, J.S., Swanson, A.A., and Norman, T.R. 'Application of the Wide-Field Shadowgraph Technique to Helicopters in Forward Flight' Journal of the American Helicopter Society, Vol. 37-No. 2, April 1992

5. Crouse Jr., G.L., Leishman, J.G., and Bi, N. 'Theoretical and Experimental Study of Unsteady Rotor/Body Aerodynamic Interactions' *Journal of the American Helicopter Society*, Vol. 37-No. 1, January 1992
6. Foley, S.M., Funk, R.B., Fawcett, P.A., and Komerath, N.M. 'Rotor-Wake-Induced Flow Separation on a Lifting Surface' *Journal of the American Helicopter Society*, Vol. 40-No. 2, April 1995
7. Brand, A., Komerath, N., and McMahan, H. 'Results from Laser Sheet Visualization of a Periodic Rotor Wake' *AIAA Journal of Aircraft*, Vol. 26-No. 5, May 1989
8. Saffman, P.G. *Vortex Dynamics* Cambridge University Press, 1992
9. Weigand, A. 'The Response of a Vortex Ring to a Transient Spatial Cut' *Proceedings of the Seventh International Symposium on Flow Visualization*. Ed. J. Crowder, Seattle, WA, September, 1995
10. Johnson, W. *Helicopter Theory* Princeton University Press, 1980
11. Marshall, J.S. 'Vortex Cutting by a Blade, Part 1: General Theory and a Simple Solution' *AIAA Journal*, Vol. 32, No. 6, June 1994
12. Kim, J.M. and Komerath, N.M. 'Summary of the Interaction of a Rotor Wake with a Circular Cylinder' *AIAA Journal*, Vol. 33, No. 3, March 1995
13. White, F.M. *Viscous Fluid Flow* McGraw-Hill, 1974
14. Lamb, H. *Hydrodynamics, Sixth Edition* Dover Publications, New York
15. Carslaw, H.S. and Jaeger, J.C. *Conduction of Heat in Solids, Second Edition* Clarendon Press, Oxford, 1959
16. Beyer, W.H., Ed. *CRC Standard Mathematical Tables, 26'th Edition* CRC Press, Boca Raton, Florida, 1981